ORIGINAL RESEARCH

An Alternative Isovelocity Surface Model for Quantitation of Effective Regurgitant Orifice Area in Mitral Regurgitation With an Elongated Orifice

Application to Functional Mitral Regurgitation

Robert D. Rifkin, MD, Shivak Sharma, MD

St. Louis, Missouri

OBJECTIVES The purpose of this study was to develop and test a simple, clinically practical alternative isovelocity surface (ISVS) model for calculating effective regurgitant orifice area (EROA) in mitral regurgitation (MR) when the regurgitant orifice is elongated, such as in functional MR.

BACKGROUND Clinical experience and 3-dimensional imaging suggest that the traditional hemispheric ISVS model used in the conventional proximal isovelocity surface area (PISA) calculation is invalid in certain MR cases and can cause erroneous EROA values.

METHODS Our ISVS model consisted of 3 sections of equal radius (R): a cylindrical midsection of length (L) positioned between 2 hemispheroidal end sections. Total ISVS area (T_S) is equal to $2\pi R^2 + \pi LR$ and EROA is equal to $(V_N/V_{CW})T_S$, where V_N is the flow velocity crossing perpendicular to the ISVS, and V_{CW} is the peak MR jet velocity by continuous-wave Doppler. This EROA was corrected for any obtuse angle, θ formed by tented leaflets, by multiplying T_S by a planar factor, $(\theta/180)$ or a combination of this planar factor for the cylindrical midsection and the solid-angle factor, $1-\cos(\theta/2)$, for the 2 spheroidal end sections. In 24 cases of severe or 3+ functional MR, we calculated EROA using 3 traditional hemispheric surfaces and 3 alternative ISVS models that differed in the leaflet angle correction applied. Results were compared with continuity-based EROA using the standard mitral valve − aortic valve stroke volume method and with predictions based upon theoretical geometric considerations.

RESULTS The mean differences between continuity EROA and ISVS area–based EROA for no angle correction, planar correction, or combined angle correction were, respectively, 0.38, 0.32, and 0.28 cm^2 for the 3 spherical surface models and 0.17, 0.018, and −0.012 cm^2 for the 3 alternative 3-section ISVS models. The empiric EROA results with both the traditional spherical and alternative ISVS models agreed well with theoretical geometric predictions.

CONCLUSIONS The traditional spherical PISA model underestimates EROA in functional MR. For elongated MR orifices, an ISVS model that mirrors orifice shape yields more accurate EROA values. Correction to the ISVS area for obtuse leaflet angulation improves accuracy of EROA estimation.   (J Am Coll Cardiol Img 2010;3:1091–1103) © 2010 by the American College of Cardiology Foundation

Echocardiography is the primary clinical method for assessing severity of mitral regurgitation (1). The proximal isovelocity surface area (PISA) technique for quantifying the effective regurgitant orifice area (EROA) is a widely accepted echocardiographic approach and has performed well in routine clinical use (1). However, it has recently been recognized that the accuracy of the EROA approach is unsatisfactory in some conditions, particularly functional mitral regurgitation (MR). Three-dimensional (3D) echocardiography suggests that the assumption of spherical isovelocity surface (ISVS) geometry, the conceptual basis of the traditional PISA calculation, may be invalid in these cases (2–4). Although 3D echocardiography may prove superior to 2-dimensional (2D) for EROA, 3D is unlikely to attain general use. Therefore, we propose a simple, modified ISVS model that better reflects the geometry of functional MR and incorporates features neglected in the current approach, yet is feasible with conventional 2D imaging systems. The proposed model comprises a cylindrical middle section mirroring the orifice elongation in functional MR and 2 hemispheric end sections. Additionally, our model includes correction for the effect on isovelocity surface area (ISVSA) of the obtuse angle typically formed by leaflet tenting in functional MR.

METHODS

Population. We screened the Barnes-Jewish Hospital Echocardiographic database from January 25, 2006, to September 15, 2009 for routinely acquired transthoracic studies with severe MR and severe left ventricular (LV) dysfunction, excluding cases with: 1) irregular rhythm; 2) more than mild aortic regurgitation; 3) intrinsic mitral valve (MV) leaflet or annular disease; or 4) inadequate image quality. This study was approved by the Washington University institutional review board.

Ultrasound equipment. A full description of the ultrasound equipment is available in the Online Appendix.

PISA radius. The ISVS radius (R) was measured in magnified apical 4-chamber MV images with color baseline shifted to Nyquist velocity 30 to 45 cm/s. Digital loops comprising 1 to 3 R-R intervals were manually cycled through systole to identify the frame with optimal timing and image quality, excluding the initial and final 2 systolic frames. Radius was measured from the color-aliasing boundary on the beam axis to the regurgitant orifice. The orifice position was identified by 2 criteria: 1) the thin neck of the color globe at the leaflet coaptation; and 2) the orifice is not posterior to the leaflet tips because flow must converge along the LV surface of the leaflets. In many cases, simultaneously acquired side-by-side magnified color and 2D MV loops (Fig. 1B) facilitated accurate orifice position identification.

Leaflet angle. The obtuse angle between the tented leaflets (arc on ventricular side of leaflets) was measured by protractor to the nearest 20° in the frame that the PISA R was measured or the adjacent simultaneous 2D noncolor frame (Fig. 1B) when available.

MR jet parameters. Continuous-wave (CW) Doppler MR jet flow profiles were planimetered for time velocity integral and peak MR velocity, V_{CW} and MR jet area (mosaic high-velocity portions only) was planimetered in the view and frame in which it was maximum, with Nyquist limits 50 to 60 cm/s.

Continuity EROA. Continuity EROA was assumed to be the gold standard for EROA (1). Details of our technique are available in the Online Appendix.

Alternative ISVS model. The 4-chamber view transects the MV commissures (leaflet edges) perpendicularly, whereas the 2-chamber view is nearly parallel to the commissures (Fig. 2, top). With tented leaflets, the commissures fail to coapt, leading to a narrow, elongated gap that forms the regurgitant orifice (Figs. 2A to 2C). We hypothesized that the ISVS in such cases differs from the traditional hemispheric model in 2 respects: 1) there is a cylindrical section lying between 2 partial spheroids that form the ends of the ISVS; and 2) flow can converge toward the orifice over the entire obtuse angle (>180°) formed by the tented leaflets; hence, the ISVS extends below the plane of the orifice until it intersects the leaflet surface.

EROA calculation. Half-pipe and hemisphere surface areas are πLR and $2\pi R^2$, respectively (L is the cylindrical section length). We tested 2 correction factors for the increased ISVSA owing to obtuse leaflet angle, θ (Fig. 2A): 1) planar angle correction = $(ISVSA)(\theta/180)$ (wedge leaflet configuration); and 2) solid angle correction = $(ISVSA)[1-\cos(\theta/180)]$ (conical leaflet configuration) (5). In contrast to acute angles (<180°), the solid angle correction factor is always greater than the planar factor for obtuse angles (Fig. 3).

We applied the planar correction factor to the cylindrical midsection of our model. We evaluated

Figure 1. Case 22 Images

(A) Zoom of 4-chamber view of tented leaflets showing isovelocity surface (ISVS) with thin neck and large mitral regurgitation (MR) jet. **(B)** Simultaneous side-by-side 4-chamber view used to locate orifice (long horizontal arrow). θ = leaflet angle; R = ISVS radius (**small single-head white arrow**). **(C)** 2-chamber view of jet shows broad MR jet originating at posterior leaflet surface. L = jet width (**black arrow**). **(D)** Magnification of **(C)** showing cylindrical convergence zone seen broadside on left ventricular (LV) side of leaflets with radius R (**short double-head black arrow**) and length ~L (**dashed black arrow**) approximately equal to width of MR jet, L (**long solid arrow LV side of leaflets**). 1-cm calibrations (**double-headed white arrows**).

the use of both factors for the model's spheroidal ends. Thus, the total ISVSA had 2 components: 1) the sum of the 2 spheroidal ends, S_S; and 2) the cylindrical midsection, S_C. Our formulas for total ISVSA, S_T, of the alternative ISVS models are:

Model 1: no angle correction: $S_T = S_S + S_C = 2\pi R^2 + \pi LR$

Model 2: planar (linear) angle correction of both sections: $S_T = S_S + S_C = (2\pi R^2 + \pi LR)(\theta/180)$

Model 3: planar angle correction in cylindrical section and solid angle correction in spherical end sections: $S_T = S_S + S_C = (2\pi R^2)[1-\cos(\theta/2)] + (\pi LR)(\theta/180)$

We also calculated S_T using the same R value but omitting the cylindrical section in 3 additional cases that represent traditional spherical ISVS models, with and without leaflet angle correction:

Model 4: no angle correction (traditional model): $S_T = S_S = 2\pi R^2$

Model 5: planar angle correction (wedge-shaped leaflet configuration): $S_T = S_S = 2\pi R^2(\theta/180)$

Model 6: solid angle correction (conical leaflet configuration): $S_T = S_S = 2\pi R^2[1-\cos(\theta/2)]$

For each model, we calculated MR EROA as:

Equation 1: MR EROA = $S_T(V_N/V_{CW})$

V_N, the flow velocity crossing perpendicular to the ISVS, is equal to the baseline-shifted color Doppler aliasing velocity (Nyquist limit) in the direction of flow. V_{CW} is the peak MR jet velocity by CW Doppler. S_T is given by models 1 to 6. Therefore, we had a total of 6 ISVS EROAs to compare with the continuity EROA.

Cylindrical section length. In MR with tented leaflets, a broad sheet of color regurgitation is observed

in the apical 2-chamber view (Fig. 1C) emerging from the posterior leaflet border along the orifice length. We measured L immediately behind the leaflets (Figs. 1C and 1D, solid black double-headed arrows), tabulating 2 values of L for each
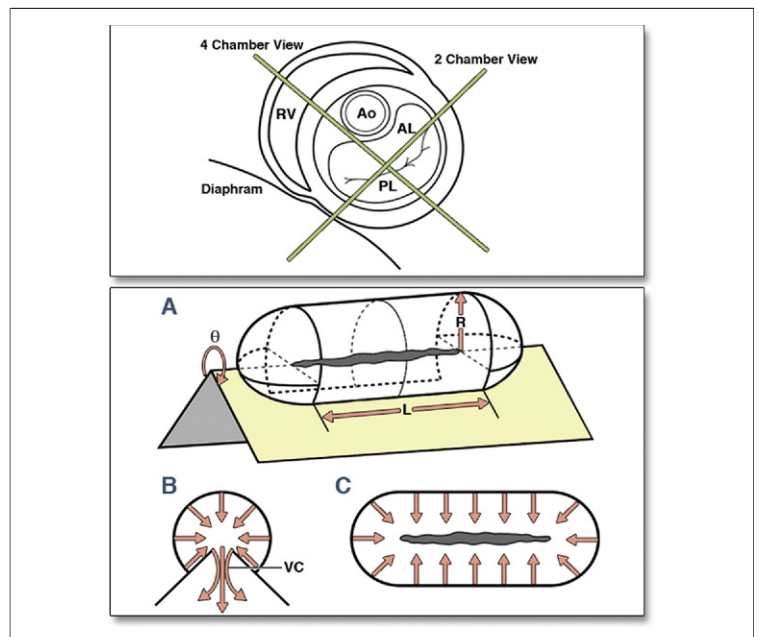
Figure 2. Proposed ISVS Model

(A) Short-axis LV cross section. Note near parallel alignment of 2-chamber view with long axis of the MV commissures/orifice and perpendicular alignment of 4-chamber view across the commissures. **(B)** Schematic of ISVS. **(C)** End-on view of model. **(D)** Superior view of ISVS. Note that the true crescent orifice shape seen in the top is shown schematically as straight to simplify the illustration. VC = vena contracta; other abbreviations as in Figure 1.

Figure 3. Angle Correction Factors

(A) Planar and solid angle factor versus θ. **(B)** Solid $-$ planar ("linear") factor versus θ. Note solid angle factor $<$ plane angle for $\theta < 180°$ but opposite for $\theta > 180°$.
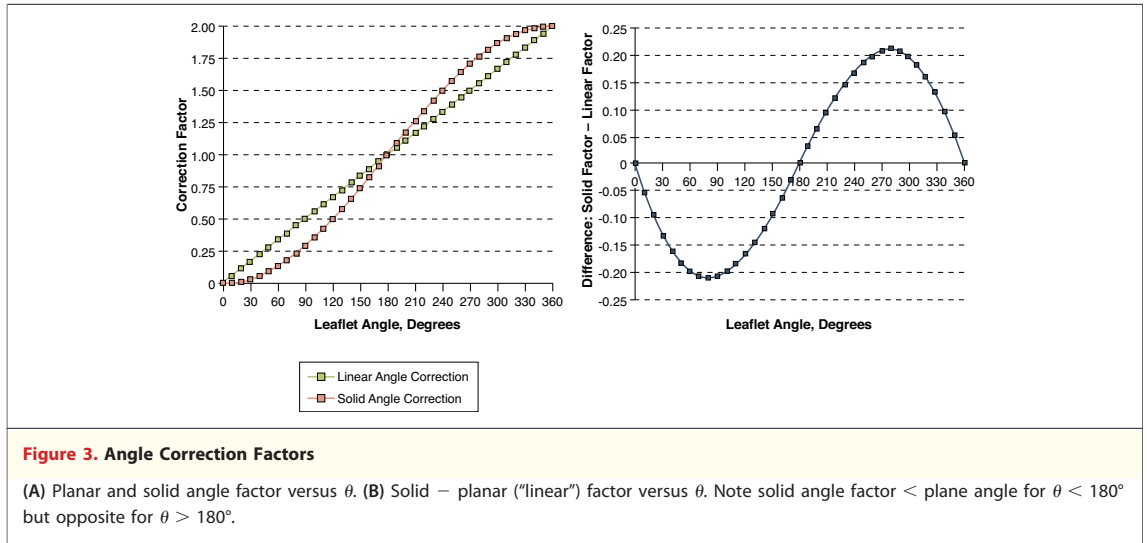
case: 1) average width in mid-systolic frames; and 2) maximum mid-systolic width.

We calculated the EROAs for models 1 to 3 using both average and maximum values of L.

Theoretical effect of cylindrical section on observed R for a given MR EROA. To determine the effect of elongated ISVS shape and obtuse leaflet angle on the aliasing R that will be observed, we used model 3's ISVSA formula for S_T with Equation 1:

$$EROA = S_T(V_N/V_{CW})$$
$$= (V_N/V_{CW})\{2\pi R^2[\cos(1-\theta/2)] + \pi RL(\theta/180)\}$$

Rearranging this equation gives:

$$2\pi[1-\cos(\theta/2)]R^2 + \pi L(\theta/180)R - (V_{CW}/V_N)$$
$$(EROA) = 0$$

Solving for R yields observed values of the ISVS radius, R_{obs}:

Equation 2: $R_{obs} =$

$$\frac{-\pi L(\theta/180) \pm \sqrt{\begin{array}{c}[\pi L\theta/180]^2 + 8\pi(EROA)\\ \times (V_{CW}/V_N)[\cos(1-\theta/2)]\end{array}}}{4\pi[\cos(1-\theta/2)]}$$

We used equation 2 to graph the expected observed R, R_{obs}, for an assumed EROA $= 0.5$ cm^2 for values of L and θ varying, respectively, between 0 to 2 cm and 180° to 270°. We assumed V_N and V_{CW} such that $2\pi(V_N/V_{CW}) = 1/2$, enabling the short-cut formula, EROA $= (R_{obs}^2)/2$, for calculating traditional PISA EROA (model 4). We graphed

these apparent EROAs over the same values of L and θ used to graph R_{obs} to determine the theoretical error caused by use of the traditional model. All measurements were made by the authors before these theoretical results, and observers were therefore blinded to the theoretical predictions.

Control cases. We calculated the EROA by traditional spherical PISA formula (model 4) and by continuity in 12 patients with the following features: 1) echo diagnosis of severe MR; 2) absent leaflet tenting; 3) ISVS zones deeper than they were wide; 4) isovelocity zone shape similar in both 4- and 2-chamber views; 5) well-defined vena contractas (VCs) of similar size in 4- and 2-chamber views; and 6) mild or less aortic regurgitation.

Statistical analysis. We tested the mean differences between continuity and model EROA across the 6 models for significance by repeated-measures analysis of variance (ANOVA) using SPSS software (SPSS, Inc., Chicago, Illinois). We used t tests to test each of the 6 mean values against zero. We employed analysis of paired differences (6,7) for method comparison between each model's EROAs and the continuity EROAs, plotting the mean and limits of agreement (± 1.96 SD) and a regression line for the difference between model and continuity EROA versus their mean values in each case for each model. We tested the significance of the means, correlation coefficients, and slopes versus zero ($H_o = 0$) by t tests (means and slopes) and T statistic for sample correlation coefficient and Fisher Z transformation (correlation coefficients). Sample size calculations and SPSS ANOVA output are available online (Online Appendix).

Table 1. Study Population Mean Values for Various Measurements (n = 24)

Measurement	Mean	SD	SE	Minimum	Maximum
EROA by continuity	0.535	0.185	0.038	0.28	0.93
Jet area (cm^2)	14.0	7.04	1.44	5.9	34.0
Jet:LA area ratio (%)	50.7	14.1	2.9	23.7	79.3
Regurgitation fraction by continuity (%)	61.8	7.8	1.6	47.6	78.2
PISA R (cm)	0.56	0.12	0.025	0.40	0.90
Leaflet angle (°)	249	16	3.3	220	290
Plane angle correction factor	1.38	0.09	0.018	1.22	1.61
Solid angle correction factor	1.56	0.11	0.023	1.34	1.82
Traditional ISVS area (cm^2)	2.05	0.94	0.192	1.01	5.09
PISA cylindrical length (cm)	1.51	0.32	0.066	0.75	2.06
Cylindrical ISVS area (cm^2)	2.65	0.89	0.182	1.38	5.05
Clinically reported LVEF (%)	21.5	10.52	2.244	10.00	63.00
V_N for ISVS area (cm/s)	37.8	7.75	1.583	28.0	64.0
V_N for MR jet area (cm/s)	56.2	6.83	1.394	45.0	72.0
Peak V_{CW} of MR jet (cm/s)	454.7	70.7	14.4	354.0	635.0

EROA = effective regurgitant orifice area; ISVS = isovelocity surface; LA = left atrial; LVEF = left ventricular ejection fraction; MR = mitral regurgitation; PISA = proximal isovelocity surface area; R = ISVS radius; V_{CW} = peak MR jet velocity by continuous wave Doppler; V_N = flow velocity crossing perpendicular to the ISVS.

RESULTS

Population composition and mean model values.
There were 17 men and 7 women, with a mean age of 65 years. Fourteen had nonischemic and 10 had ischemic cardiomyopathy. The mean LV ejection fraction was 22%. Other important mean values related to the ISVS models and image acquisition settings are shown in Table 1. It is noteworthy that the mean cylindrical section ISVSA (2.65 cm^2, row 11) was approximately 56% of the mean total ISVSA (2.65/[2.65+2.05], row 9).

MR jet characteristics. Jet geometry measurements relevant to MR severity are shown in Table 1 (rows 2 and 3). Additional jet features are available in the Online Appendix.

ISVS EROA versus continuity EROA. The 3 spherical models (models 4 to 6) produced the smallest EROAs in all cases (Table 2 and Fig. 4, bars 1 to 3,

each case) and the largest differences from continuity EROA (Table 2 and Figs. 5A and 5B, bars 1 to 3).
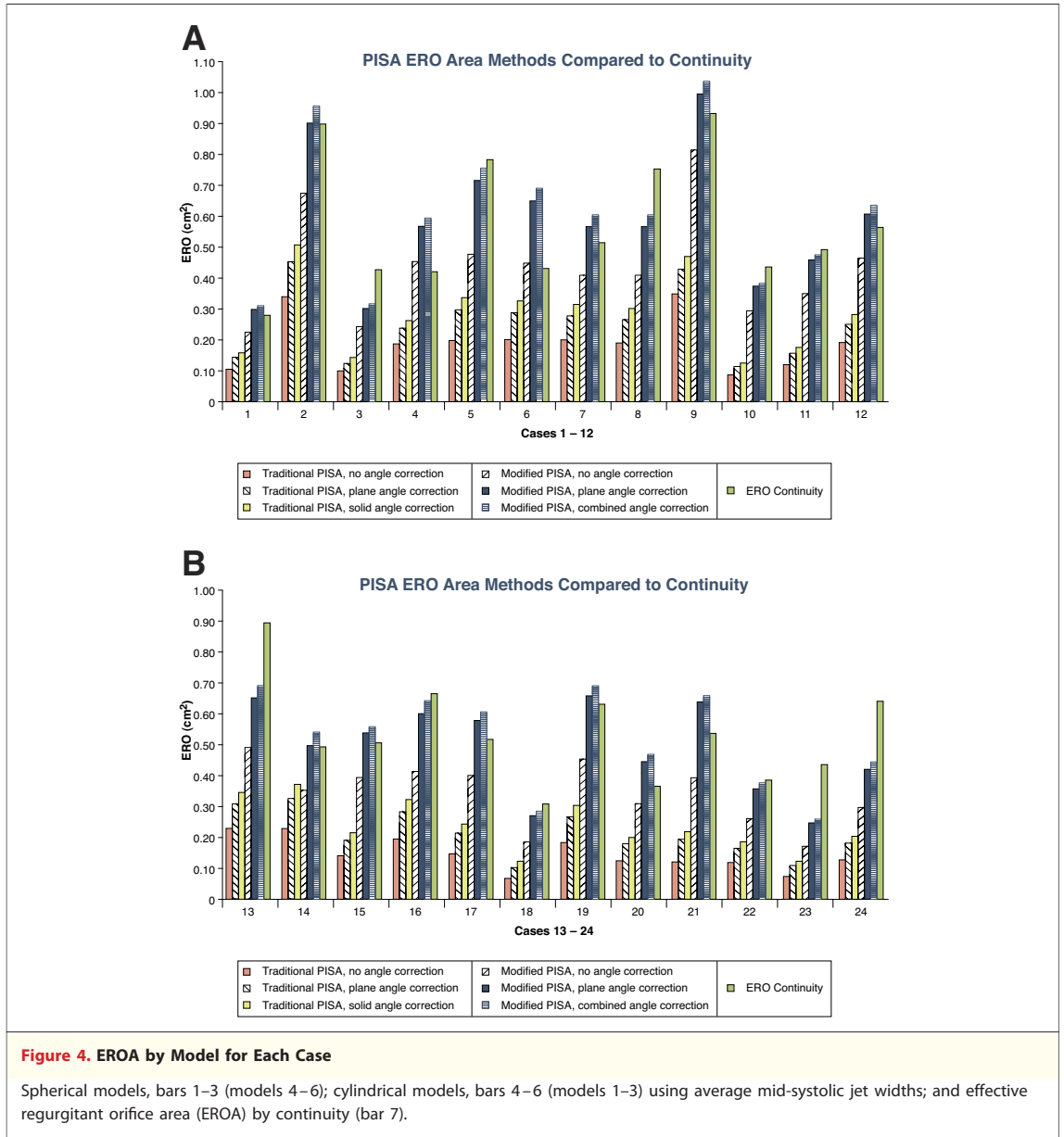
Mean EROA differences from the continuity EROA (Fig. 5C) among the 6 models were significant (p = 0.0016, ANOVA). Angle compensation alone did not adequately correct spherical model deviation from continuity EROA (Figs. 5A and 5B, bars 2 and 3 in each case; Fig. 5C, models 5 and 6 in bars 2 and 3). Smaller but persistent differences were noted for the new model without angle-correction (Fig. 5C, model 1, bar 4). However, when both L and the obtuse leaflet angle are accounted for, either using planar or combined angle correction (Fig. 5C, models 2 and 3, bars 5 and 6), the disparity with continuity EROA was small.

Use of the maximum, instead of the mean, 2-chamber jet width slightly worsened agreement

Table 2. Mean Values of EROA, RV by Continuity and PISA, and Mean Differences Between Continuity and PISA EROA and RV

Method	Mean EROA (cm^2; n = 24)	SD	SE	Continuity EROA − PISA EROA	SD	SE	Mean RV (ml; n = 24)	SD	SE	Continuity RV − PISA RV	SD	SE
MR EROA by continuity	0.556	0.185	0.038				73	18	4			
Traditional spherical PISA												
EROA—no angle correction factor	0.169	0.073	0.015	0.387	0.136	0.028	21.92	7.51	1.53	50.74	14.45	2.95
PISA EROA—linear correction	0.232	0.094	0.019	0.324	0.125	0.026	30.13	9.71	1.98	42.53	13.83	2.82
PISA EROA—solid correction	0.261	0.105	0.021	0.295	0.121	0.025	33.97	10.89	2.22	38.69	13.71	2.80
New cylindrical model PISA												
EROA—no angle correction factor	0.391	0.145	0.182	0.165	0.111	0.023	51.02	14.79	3.02	21.64	13.54	2.76
PISA EROA—linear correction	0.538	0.185	0.038	0.018	0.114	0.023	70.23	19.07	3.89	2.43	14.60	2.98
PISA EROA—solid correction	0.568	0.195	0.040	−0.012	0.117	0.024	74.07	20.02	4.09	−1.41	14.92	3.05

RV = regurgitation volume; other abbreviations as in Table 1.

Figure 4. EROA by Model for Each Case

Spherical models, bars 1–3 (models 4–6); cylindrical models, bars 4–6 (models 1–3) using average mid-systolic jet widths; and effective regurgitant orifice area (EROA) by continuity (bar 7).
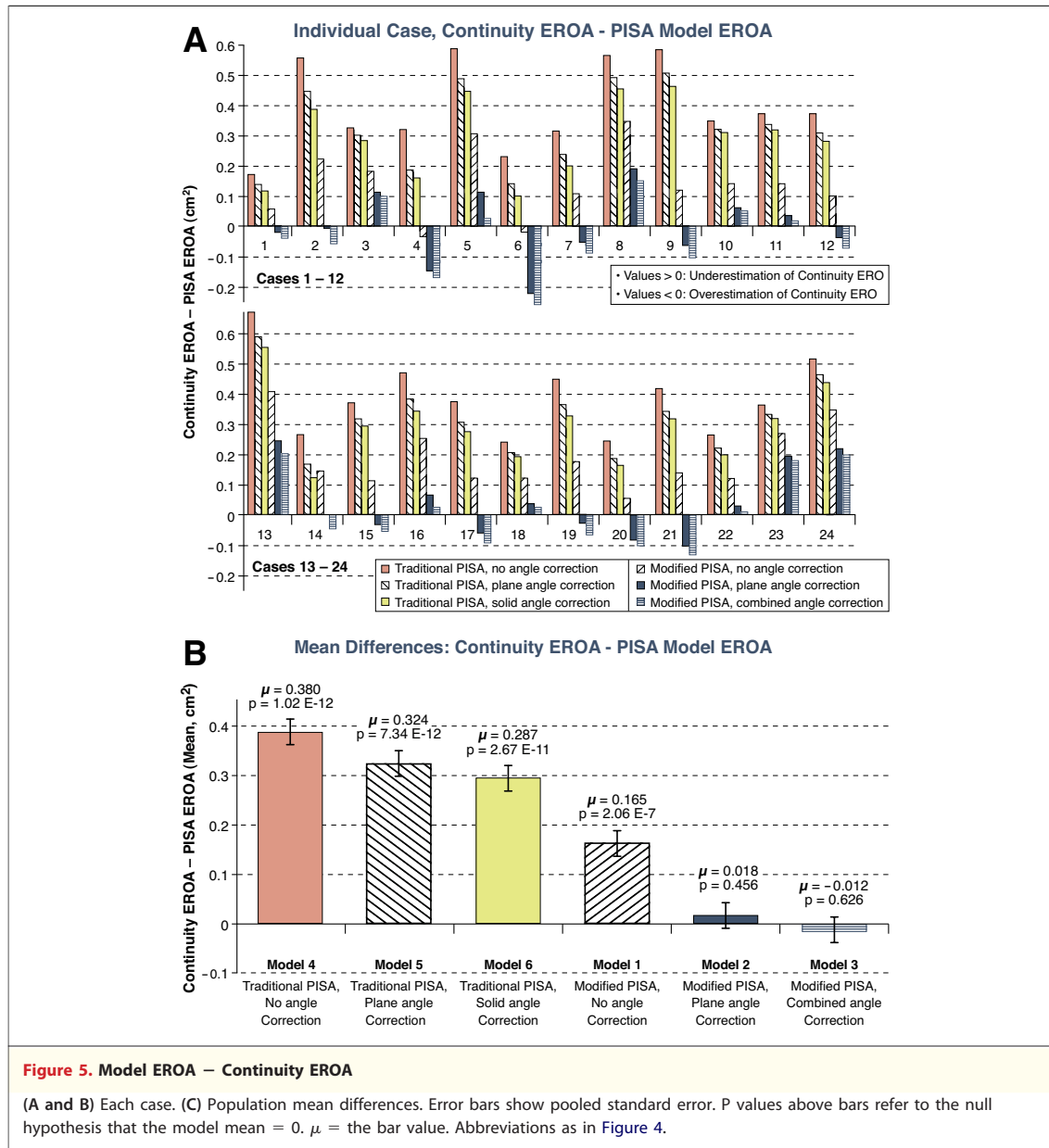
with continuity EROA for models 2 and 3 (differences from continuity = −0.019 and −0.049 cm² vs. +0.018 and −0.012 shown above bars 5 and 6, respectively; Fig. 5C). Model 1 improved, but only slightly (difference = 0.138 vs. 0.165 shown above bar 4; Fig. 5C).

The variation in the mean differences (continuity EROA − model EROA) across the 6 models was significant (p < 0.00001) by repeated-measures ANOVA under either Greenhouse-Geisser, Huynh-Feldt, or lower-bound corrections. Detailed ANOVA results are available in the Online Appendix.

Paired-difference analysis (Fig. 6) also showed that the mean difference between model and

continuity EROA was significant for all traditional models (models 4 to 6; p ≤ 0.023) but not significant for the alternative models (models 1 to 3; p ≥ 0.15). Similarly, regression slopes differed significantly from zero for all 3 traditional models (p < 0.000001) but not for the alternative models, indicating the absence of influence of EROA magnitude on accuracy only for the alternative models, particularly models 2 and 3 that included angle correction. The correlation between model and continuity EROA for model 2 was 0.823 (Fig. 7).

Qualitative severity classification. Traditional spherical PISA misclassified many cases as mild or

Figure 5. Model EROA − Continuity EROA

(A and B) Each case. (C) Population mean differences. Error bars show pooled standard error. P values above bars refer to the null hypothesis that the model mean = 0. μ = the bar value. Abbreviations as in Figure 4.
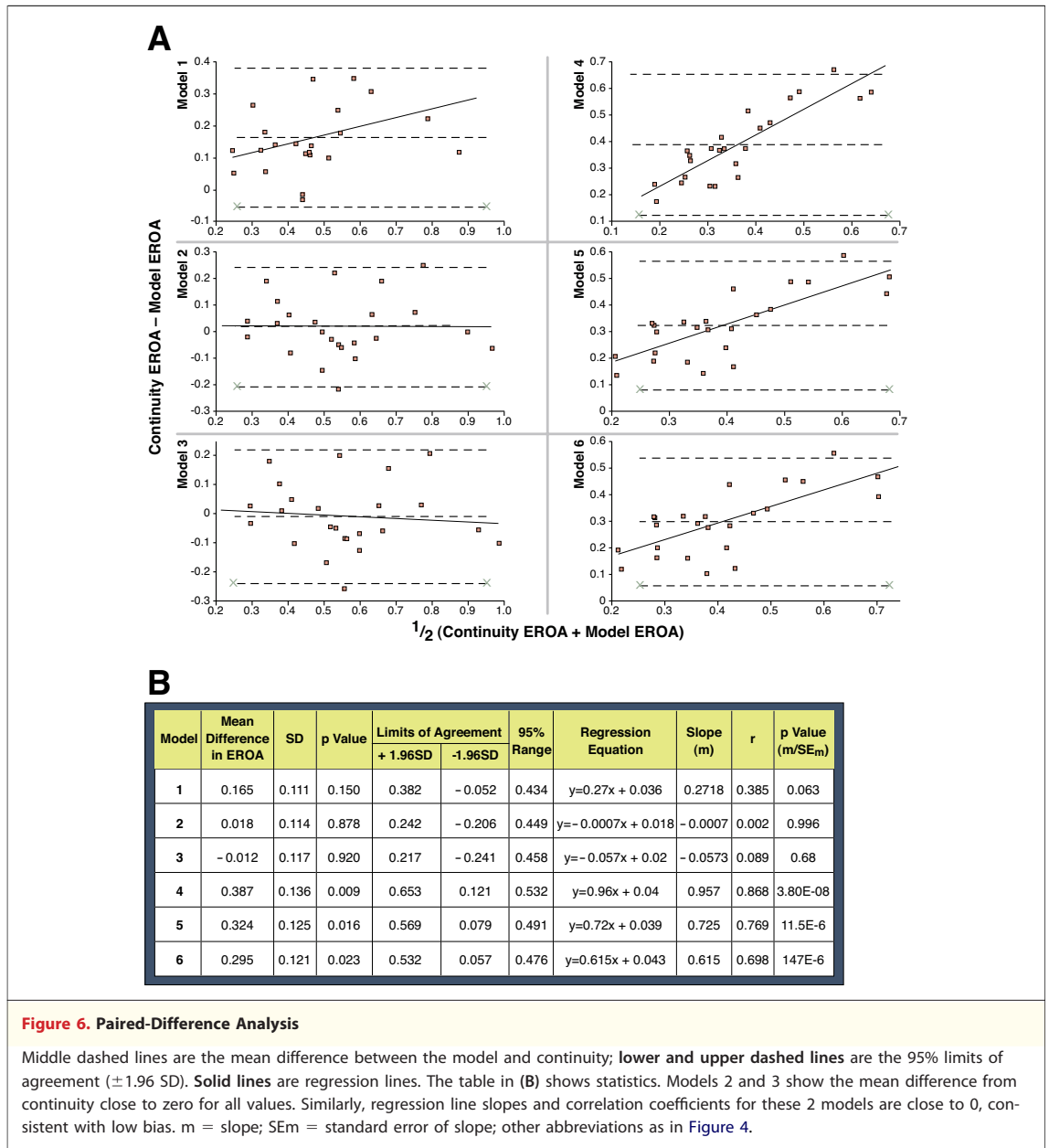
moderate, despite leaflet angle correction (Table 3). The cylindrical model without angle correction moderately improved classification; however, with leaflet angle correction, classification accuracy almost matched classification of continuity EROA.

Theoretical predictions. With either leaflet tenting or orifice elongation, theory predicts a reduction in R (Fig. 8A). For the case of a true orifice area of 0.5 cm^2 (severe MR), for $\theta = 270°$, and L = 0, R will be approximately 0.76 cm instead of 1 cm. With orifice elongation also present (L > 0), R falls further. For L = 1 cm and $\theta = 240°$, R will be approximately 0.63 cm rather than 1 cm. This

reduced R results in underestimation of the EROA to approximately 0.19 cm^2 when it is used in spherical models to calculate EROA (Fig. 8B). Even when the ISVS is spherical (L = 0), the obtuse leaflet angle results in reduced R and EROA underestimation (y-axis intersections, Figs. 8A and 8B, respectively).

Figure 9 generalizes Figure 8, top, showing percent R changes for various orifice areas from 0.2 to 0.6 cm^2.

Control cases. The EROAs by traditional spherical PISA, 0.61 cm^2, and Doppler continuity, 0.65 cm^2, agreed closely (Table 4, rows 1 and 2). Mean PISA R was 1.18 cm (Table 4, row 6). Other parameters

A

Continuity EROA – Model EROA

¹/₂ (Continuity EROA + Model EROA)

B

Model	Mean Difference in EROA	SD	p Value	Limits of Agreement		95% Range	Regression Equation	Slope (m)	r	p Value (m/SEₘ)
				+ 1.96SD	-1.96SD					
1	0.165	0.111	0.150	0.382	– 0.052	0.434	y=0.27x + 0.036	0.2718	0.385	0.063
2	0.018	0.114	0.878	0.242	– 0.206	0.449	y=– 0.0007x + 0.018	– 0.0007	0.002	0.996
3	– 0.012	0.117	0.920	0.217	– 0.241	0.458	y=– 0.057x + 0.02	– 0.0573	0.089	0.68
4	0.387	0.136	0.009	0.653	0.121	0.532	y=0.96x + 0.04	0.957	0.868	3.80E-08
5	0.324	0.125	0.016	0.569	0.079	0.491	y=0.72x + 0.039	0.725	0.769	11.5E-6
6	0.295	0.121	0.023	0.532	0.057	0.476	y=0.615x + 0.043	0.615	0.698	147E-6

Figure 6. Paired-Difference Analysis

Middle dashed lines are the mean difference between the model and continuity; **lower and upper dashed lines** are the 95% limits of agreement (±1.96 SD). **Solid lines** are regression lines. The table in **(B)** shows statistics. Models 2 and 3 show the mean difference from continuity close to zero for all values. Similarly, regression line slopes and correlation coefficients for these 2 models are close to 0, consistent with low bias. m = slope; SEm = standard error of slope; other abbreviations as in Figure 4.

support the presence of severe MR in these cases. The correlation between the LV stroke volume (SV) by Doppler continuity and the PISA MR was 0.73.

DISCUSSION

Main findings. Our principal findings were: 1) in functional MR, the traditional hemispheric ISVS model underestimated the true ISVSA, resulting in marked underestimation of the EROA; 2) an elongated ISVS model consisting of a simple cylinder flanked on both sides by spheroids having R identical to the cylinder improved EROA estimation;

and 3) correction to the resulting combined ISVSA for the increased flow owing to the obtuse angle formed by tented leaflets in functional MR may be necessary to accurately estimate the EROA with either model.

Accuracy of new model. Despite moderate case-to-case variation in quantitative accuracy of the new model (Figs. 5A and 5B), agreement of mean values with Doppler continuity was very good (Fig. 5C). Moreover, in the individual cases, the new model produced the closest quantitative estimates and best qualitative classification of severity compared with the Doppler continuity
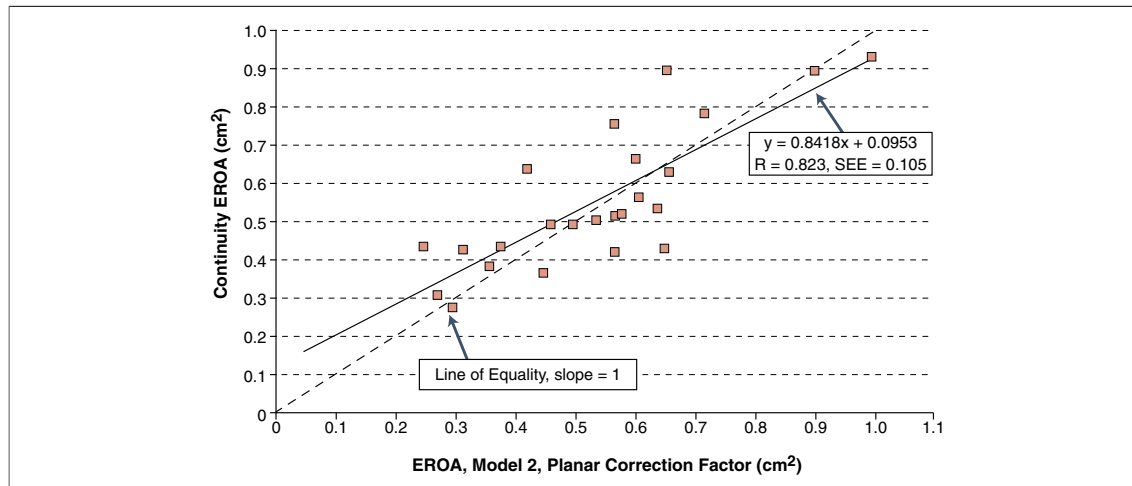
Figure 7. Conventional Regression for Continuity EROA on to Cylindrical Model EROA for Model 2

The correlation 0.823 was good, the standard error (SEE) was modest in magnitude, regression slope was near 1, and the regression line was very close to the line of unity. Abbreviations as in Figure 4.

reference. This superiority obtained despite angle correction of spherical models (Fig. 5C, bars 2 and 3).

We also found good agreement between theoretical and measured values of ISVS L and R. Theory showed that for a given EROA, R falls substantially as the orifice lengthens and tenting worsens. This may explain why Grigioni et al. (8) reported that adverse event rates in functional MR begin to increase at EROA $= 0.2$ cm^2 versus 0.4 cm^2 in other forms of MR. The EROAs based on average 2-chamber apical view mid-systolic MR jet width agreed with continuity-EROAs slightly better than when the maximum width was used.

MR jet area. The MR jet to left atrial (LA) area ratio performed as well in classification of MR severity as our new method (Table 3) and far superior to the

traditional PISA model. This could be due partly to the use of consistent Nyquist limits and other machine settings in our lab for recording MR jets and partly to our highly selected study population.

Angle correction factor. In contrast to mitral stenosis (5), angle correction has been neglected in the application of the PISA method for MR (9). However, computational and in vitro tank models have been used to analyze the effect of angulation on traditional PISA-based area estimates for regurgitation through circular orifices at the apex of inverted funnels (10,11). Cape et al. (10) used a tank model of MR with funnel-shaped obtuse inflow angles up to 270° and reported that, compared with a flat (180°) surface, PISA R decreased progressively as the obtuse inlet angle increased. The solid angle factor, $1-\cos(\theta/2)$, accurately corrected their ISVSAs. In contrast, using a similar tank model, Giesler et al. (11) found the empirically measured correction factor was less than $1-\cos(\theta/2)$. The reduction increased for small orifices and proximity to the orifice. For example, with a 7-mm diameter, 240° funnel orifice (area $= 0.4$ cm^2 corresponding to 3+ MR), and at 10 to 12 mm from the orifice (typical color isovelocity shell R for this size orifice), the empiric correction factor was approximately 1.3 instead of 1.5 given by $1 - \cos(\theta/2)$. Thus, the solid angle factor could result in a 15% overestimation (1.5/1.3) of orifice area for a circular orifice.

Previous alternative ISVS models. Matsumura et al. (4) developed customized software using 7 measurements of the 3D color MR Doppler field to

Table 3. Classification of MR Severity by Method

Method	MR Severity		
	Mild	Moderate	Severe
EROA by continuity	0	4	20
Jet area ratio	0	6	18
Spherical PISA model			
No angle correction	19	5	0
Planar correction	11	11	2
Solid correction	7	15	2
Cylindrical PISA model			
No angle correction	2	10	12
Planar correction	0	6	18
Solid correction	0	6	18

Abbreviations as in Table 1.
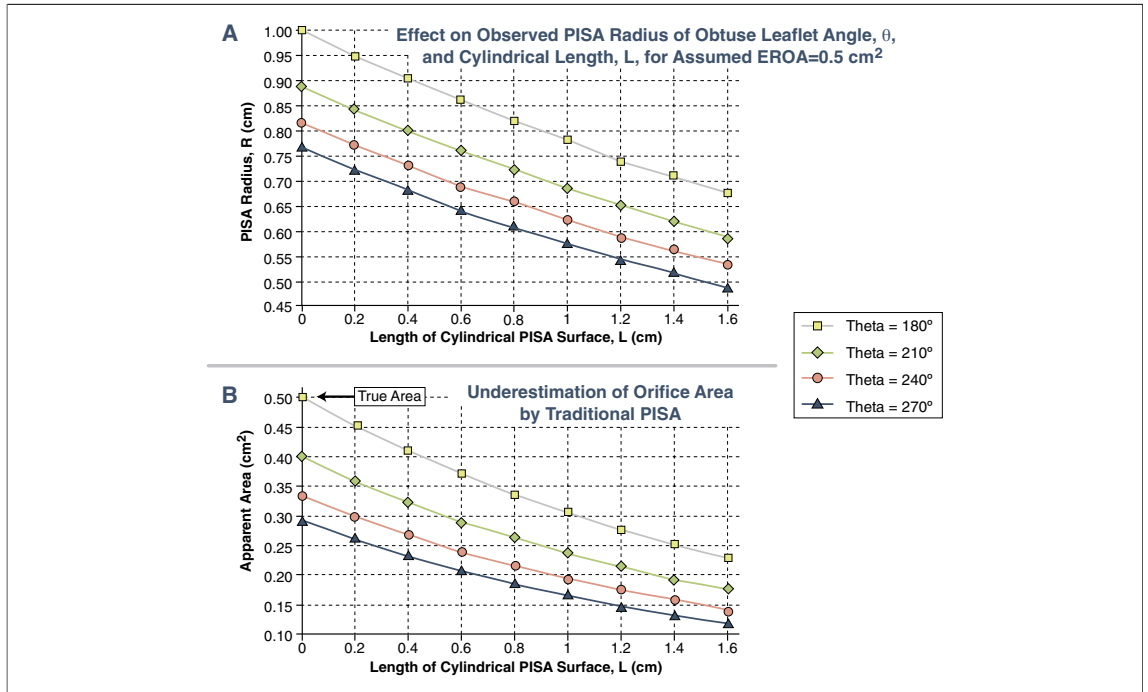
Figure 8. Theoretical Predictions

Assumed true EROA = 0.5 cm^2. **(A)** Predicted observed ISVS R for 4 values of θ and L from 0 to 2 cm. **(B)** Apparent EROA using spherical model and predicted observed values of R from top graph. PISA = proximal isovelocity surface area; other abbreviations as in Figs. 1 and 4.

reconstruct the ISVS as a collection of discrete triangular facets and numerically computed their area. Its shape tended to be hemiellipsoidal. This complex model required specialized hardware and software, yet only reduced the EROA underestimation from 49% in the traditional hemispheric model to 26% when compared with the Doppler continuity EROA.

The present study was motivated by an interest in developing a model that would be practical for routine clinical use on standard ultrasound equip-

ment. Our parametric model meets this objective; in this initial investigation, its performance appears similar or superior to that of Matsumura et al. (4). It is unclear whether their program inherently corrected for obtuse leaflet angles; however, if not, this could explain our improved results. In this regard, it is of interest that when we omitted angle correction from our model (Fig. 5C, bar 4), mean underestimation of continuity EROA was 29.5% (0.165/0.56), a value similar to the 26% underestimation reported by Matsumura et al. (4), suggesting

Table 4. Control Case Mean Values for Various Measurements (n = 12)

Measurement	Mean	SD	SE	Minimum	Maximum
EROA by continuity (cm^2)	0.655	0.201	0.058	0.35	1.02
EROA by traditional PISA model (cm^2)	0.613	0.159	0.046	0.43	0.92
Jet area (cm^2)	16.8	9.04	2.86	7.1	35.0
Jet:LA area ratio (%)	51.0	10.9	3.4	35.7	69.1
Regurgitation fraction by continuity (%)	62.6	8.2	2.4	47.0	74.3
PISA R (cm)	1.18	0.23	0.066	0.76	1.50
V_N for PISA (cm/s)	36.5	10.16	2.932	29.0	67.0
Peak V_{CW} of MR jet (cm/s)	508.9	51.66	14.914	395.0	572.0
Continuity MV SV (ml)	157.8	44.58	12.869	98.0	234.2
PISA LV SV (ml)	152.7	47.18	13.620	100.4	237.4

MV = mitral valve; SV = stroke volume; other abbreviations as in Table 1.
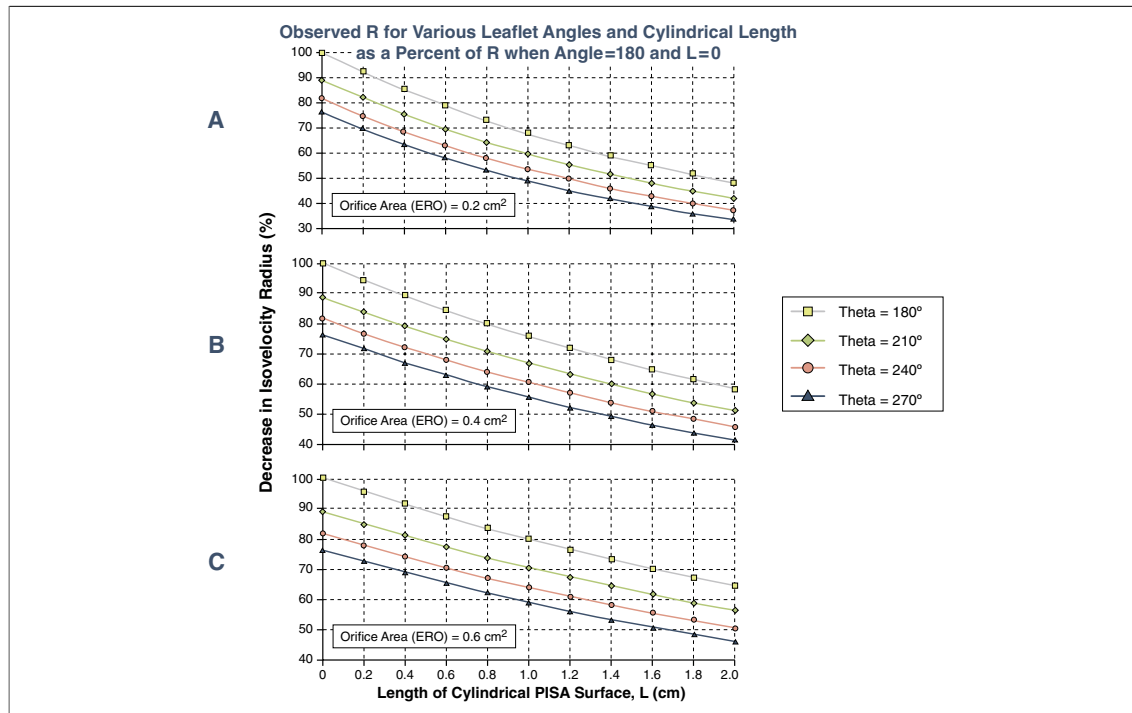
Figure 9. Generalization of Figure 8

Using the same range of L and θ as in Figure 8, the percent changes in observed R are shown for EROAs 0.2 (**A**), 0.4 (**B**), and 0.6 cm^2 (**C**). When L = 0, the percent changes owing to tenting angle, θ, are independent of the true orifice area. The reduction in EROA estimate if a spherical model is used will be equal to the square of the fractional reduction in R. Thus, if measured R is 70% of the value it would be for a circular orifice of the same area, the EROA estimate will be 49% (0.7^2) of the true EROA. Abbreviations as in Figs. 1 and 4.

that their numeric method may not have corrected for leaflet angle.

Basis for elongated ISVS model. The need for an axially asymmetric ISVS model relates to its proximity to the orifice. Were it sufficiently remote from the orifice, the ISVS would be spheroidal regardless of orifice shape. However, with lower Nyquist aliasing thresholds, an expanded ISVS would collide with tissue boundaries and overlap LV outflow, distorting its shape. Additionally, excessive low Nyquist color noise would obscure the isovelocity color boundary. Thus, at practical Nyquist thresholds, the ISVS model for an asymmetric orifice may need to mirror orifice shape more closely. This implies that the interpreter must assess from image features whether a cylindrical or spherical model should be used to compute the EROA. Our results imply that the ISVS with our alternative geometry is far enough from an elongated orifice that minor irregularities in orifice width along its length and its crescentric shape (Fig. 2, top) do not distort the ISVS shape significantly (Figs. 2A to 2C).

Elliptic versus cylindrical ISVS shape. Unlike a sphere or cylinder, the surface area of a general ellipsoid cannot be expressed by an exact algebraic function

(12). Thus, elliptic models may require numeric reconstruction of the ISVS, rendering them impractical for clinical use. By contrast, the simplicity of our model lends itself to a simple shortcut for EROA when the Nyquist limit (V_N) is approximately 40 cm/s and MR peak velocity (V_{CW}) is approximately 5 m/s:

$$EROA = (2\pi R^2 + \pi RL)(V_N/V_{CW}) = \pi R(2R+L)$$
$$\times(V_N/V_{CW}) \sim R^2/2 + RL/4$$

Accordingly, addition of the term RL/4 provides the ISVSA of an elongated orifice for this special case of V_N and V_{CW}. The obtuse angle correction can then be applied for the final EROA estimate. Thus, for planar angle correction in all model sections:

$$EROA \sim (R^2/2 + RL/4)(\theta/180)$$

Vena contracta. Our study suggests that the vena contracta (VC) measurement must be used cautiously for severity assessment in functional MR. With orifice elongation, a scan plane not precisely perpendicular to the orifice may produce a factitiously large VC. The true VC is seen only in the plane precisely perpendicular to the long axis of the orifice and may be misleadingly small (Fig. 2C). Geometric considerations using a rectangular or elliptic shape to model the elongated orifice show

that for EROAs of 0.3 to 0.5 cm^2 and L of 1.0 to 2 cm, the VC seen exactly end-on in the plane perpendicular to the long axis of the orifice (Fig. 2B) would measure between 75% and 25%, respectively, of that with a circular orifice of identical ERO. In our retrospective series, images were not optimized for VC. Therefore, we omitted this indicator of MR severity from the analysis.

Pitfalls in use of the cylindrical model. Just as the spherical ISVS model may cause underestimation of EROA when applied to an elongated orifice, the cylindrical model can cause overestimation of EROA if applied to a circular orifice, the magnitude of which is approximately RL/4. Therefore it is important to recognize the presence of an elongated orifice and to avoid applying the cylindrical model when features of significant orifice elongation are absent. Potentially, this source of error could be removed by subtracting the 4-chamber view VC dimension from the 2-chamber broadside jet length and using this value for L in the cylindrical model, but we did not investigate this approach in the present study. However, correction for obtuse leaflet angle, if present, may still improve accuracy even in the setting of a circular or nearly circular orifice.

Recognizing orifice elongation. Elongation is suggested in a 2-chamber view by a wide central band of free regurgitation perpendicular to the valve plane, appearing to originate along the posterior leaflet surface without a visible VC. A narrow band of color reversal parallel to the valve leaflet plane is seen on the LV side of the leaflet surface, similar in depth to the 4 chamber ISVS radius R (corrected for Nyquist differences) and length similar to the color MR jet width, L, on the LA side (Figs. 1C and 1D). This band represents the cylindrical ISVS seen broadside.

In a 4-chamber view, with a circular orifice and spherical ISVS, the color-aliased zone is as deep as, or deeper than, it is wide, and its width tapers near the orifice. By contrast, when the orifice is elongated, the aliased zone tends to be wider than it is deep owing to scan plane obliquity off the perpendicular with the commissure. This shape, and the relatively shallow size of the zone for the MR jet area, are often mistakenly attributed to technical factors, but they actually reflect the elongated ISVS shape. However, the width of the isovelocity zone will generally be smaller in the 4- than in the 2-chamber view, whereas the dimensions of the zones are similar in both views with a circular orifice and spheroidal zone. Finally, the 4-chamber VC, if carefully imaged, will be much narrower than the minimum width of the MR jet seen in the 2-chamber view at the leaflet.

Study limitations. Systematic overestimation of the MV SV or underestimation of ISVS R could cause the traditional PISA method to appear to underestimate continuity-based MR EROA. Identifying orifice location is often challenging, allowing both underestimation and overestimation of ISVS R. However, because flow must converge along the leaflet's ventricular surface, the orifice cannot be behind this surface. Importantly, our theoretical predictions of expected ISVS R with elongation and leaflet tenting agreed closely with our empiric R measurements, and our control series PISA EROA agreed well with their corresponding continuity EROAs, validating our measurement technique and supporting the absence of systematic errors in our ISVS R measurements.

The major potential source of overestimation of MV SV is mitral annular diameter. Our mean diameter was 3.3 cm. Mihalatos et al. (13) reported that the MV orifice becomes circular and its diameter increases progressively with MR severity. They found mean end-systolic and end-diastolic diameters of 1.95 cm/m^2 and 1.86 cm/m^2, respectively, in 19 severe MR cases. For an average adult body surface area of approximately 1.7 m^2, this equates to a diameter of approximately 3.23 cm (1.9 × 1.7), in close agreement with our measurements. Moreover, our mean Doppler continuity EROA, 0.55 cm^2, and regurgitant fraction, 61.5%, are not unusually large and are highly consistent with the mean jet to LA area ratio, 50.7%. These findings suggest that overestimation of continuity-based EROA by overmeasurement of MV orifice diameter was unlikely in our series.

Our study was retrospective with a small population size. Because we had theoretical model–predicted values that we generated after all measurements were made, we treated them as a proxy for image blinding and observer variability studies. The close agreement between our theoretical and empiric values strongly supports accuracy of our measurements for both continuity MR SV and ISVS R and mitigate these limitations. Accuracy of the new model in cases with more normal LV function and/or significantly less leaflet tenting and MR was not established in this study.

CONCLUSIONS

Our findings add insight to the ISVS methodology in MR but also introduce additional complexity that will require greater attention in image acquisition and interpretation. The popular conception of the PISA method, based on a hemisphere, appears to be an oversimplification. It is necessary for the interpreter to

assess image features and select the appropriate model to apply. Image acquisition protocols may need revision to bring out these features more clearly. In particular, magnified MV images should be obtained in 4- and 2-chamber views in color and 2D modes, with attention given to recording the shape of the flow convergence zones in both views.

When the ISVS R > 1 cm in any view (with Nyquist ~40 cm/s and peak MR velocity ~5 m/s), MR is likely to be severe. But when R < 1 cm, careful scrutiny of the orthogonal plane will be necessary to assess whether an elongated or spherical model is appropriate to calculate EROA. We note that that 10 of our 24 cases carried an ischemic cardiomyopathy diagnosis, suggesting that our model may be applicable in more than one etiology of MR. The alternative model clarifies the not uncommon cases in which the traditional PISA EROA calculation appears too small for the size of the color flow Doppler MR jet.

Finally, our data suggest that angle correction should be employed for final calculation of EROA regardless of which model is used. The simple planar correction appears satisfactory. However, more data are needed to verify the need for and especially the correct magnitude of angle correction given the differences reported in the literature cited.

Reprint requests and correspondence: Dr. Robert D. Rifkin, Division of Cardiology, Washington University School of Medicine, Campus Box 8086, 660 South Euclid Avenue, St. Louis, Missouri 63110. *E-mail: rrifkin@dom.wustl.edu.*

REFERENCES

1. Zoghbi WA, Enriquez-Sarano M, Foster E, et al. Recommendations for evaluation of the severity of native valvular regurgitation with two-dimensional and Doppler echocardiography. J Am Soc Echocardiogr 2003;16:777–802.

2. Iwakura K, Ito H, Kawano S, et al. Comparison of orifice area by transthoracic three-dimensional Doppler echocardiography versus proximal isovelocity surface area (PISA) method for assessment of mitral regurgitation. Am J Cardiol 2006;97:1630–7.

3. Yosefy C, Levine RA, Solis J, et al. Proximal flow convergence region as assessed by real-time 3-dimensional echocardiography: challenging the hemispheric assumption. J Am Soc Echocardiogr 2007;20:389–96.

4. Matsumura Y, Saracino G, Sugioka K, et al. Determination of regurgitant orifice area with the use of a new three-dimensional flow convergence geometric assumption in functional mitral regurgitation. J Am Soc Echocardiogr 2008;21:1251–6.

5. Rifkin RD, Harper K, Tighe D. Comparison of proximal isovelocity surface area method with pressure half-time and planimetry in evaluation of mitral stenosis. J Am Coll Cardiol 1995;26:458–65.

6. Bland JM, Altman DG. Difference versus mean plots. Ann Clin Biochem 1997;34:570–1.

7. Zou KH, Tuncali K, Silverman SG. Correlation and simple linear regression. Radiology 2003;227:617–22.

8. Grigioni F, Enriquez-Sarano M, Zehr KJ, et al. Ischemic mitral regurgitation: long-term outcome and prognostic implications with quantitative Doppler assessment. Circulation 2001;103:1759–64.

9. Oh JK, Seward JB, Tajik AJ. The Echo Manual. Philadelphia, PA: Lippincott Williams & Wilkins, 2006.

10. Cape EG, Thomas JD, Weyman AE, Yoganathan AP, Levine RA. Three-dimensional surface geometry correction is required for calculating flow by the proximal isovelocity surface area technique. J Am Soc Echocardiogr 1995;8:585–94.

11. Giesler M, Stein M, Grossmann G, et al. Influence of the orifice inlet angle on the velocity profile across a flow convergence region by color Doppler in vitro. Echocardiography 2000;17:419–28.

12. Wikipedia. Ellipsoid. Available at: http://en.wikipedia.org/wiki/Ellipsoid. Accessed September 10, 2010.

13. Mihalatos DG, Joseph S, Gopal A, et al. Mitral annular remodeling with varying degrees and mechanisms of chronic mitral regurgitation. J Am Soc Echocardiogr 2007;20:397–404.

Key Words: EROA ▪ functional mitral regurgitation ▪ isovelocity surface ▪ mitral regurgitation ▪ PISA.

▶ **APPENDIX**

For expanded Methods, Results, and Discussion sections, please see the online version of this article.